Sensors and Actuators B 187 (2013) 301–307

Contents lists available at SciVerse ScienceDirect

Sensors and Actuators B: Chemical

journal homepage: www.elsevier.com/locate/snb

Synthesis and gas sensing properties of hierarchical SnO_2 nanostructures

Peng Sun, Xiaodong Mei, Yaxin Cai, Jian Ma, Yanfeng Sun, Xishuang Liang*, Fengmin Liu, Geyu Lu

State Key Laboratory on Integrated Optoelectronics, College of Electronic Science and Engineering, Jilin University, Changchun 130012, People's Republic of China

ARTICLE INFO

Article history:
Available online 23 November 2012

Keywords:
Hydrothermal synthesis
SnO_2
Hierarchical nanostructures
Gas sensor

ABSTRACT

A low-cost and environmentally friendly hydrothermal route to the synthesis of hierarchical SnO_2 nanostructures was described. The structure and morphology of the as-prepared product were characterized by various characterization techniques. The results revealed that these nanostructures were built from two-dimensional (2 D) nanosheets with the thicknesses of about 8 nm. Moreover, the amount of hydrochloric acid played a crucial role in the control of the final size and morphology of product. Gas sensors based on hierarchical SnO_2 nanostructures were fabricated, and their gas sensing properties were tested for response to ethanol, acetone, formaldehyde, CO, toluene, H_2 and H_2S gases. The sensor showed excellent selectivity toward ethanol. At an ethanol concentration of 100 ppm, the response of the hierarchical SnO_2 nanosheets was about 33, which was about 2.5 times higher than that of the nanoparticles. The response time of the sensor to 60 ppm ethanol was shorter than 11 s at the optimal operating temperature of 275 °C. The enhancement in gas sensing properties was attributed to their unique structures.

1. Introduction

It is well known that the most important aspect of investigation of gas sensors based on semiconductor oxides is its sensitivity, selectivity, and stability. Therefore, many studies have been conducted in order to improve the performance of gas sensors by using crystallites with reduced dimensions since Yamazone demonstrated that a reduction in crystallite size can significantly increase sensor performance [1]. Indeed, smaller particle size has been found to result in improved gas responses [2–4]. However, the aggregation between the nanoparticles becomes very strong because the Van der Waals attraction is inversely proportional to the particle size. Under this configuration, a high sensitivity can't be achieved because the change in resistance occur only the surface region. Great efforts have been made to alleviate the above-mentioned drawback of the aggregation. The synthesis of sensing materials with novel structure is one of the most promising solutions because they can be achieved easily. In this respect, the low dimension (nanorods, nanowires, and nanoplates) and mesoporous oxide structures have been used to improve gas sensing characteristics [5–9], due to a less agglomerated configuration. Among them, hierarchical structures, the higher dimension of a micro- or nanostructure assembled from low dimensional nanosized building blocks, have attracted considerable attention due to their low density, large surface area, and surface permeability. These structural features are beneficial to the diffusion and reaction of test gas.

Tin dioxide (SnO_2), as an n-type wide-band gap ($E_g = 3.6$ eV) semiconductor, is one of most intensively studied materials due to its widely important applications such as gas sensors, solar cells, and photovoltaics [10–14]. It is well known that both the size and morphology of semiconductor oxides have a significant impact on their properties. The unique morphology and structure may display new properties and promising applications in many fields. Therefore, over the past decades, several groups have synthesized SnO_2 micro- and nanostructures with different morphologies by various preparation routes, including vapor phase growth [15], hydrothermal reaction [16–18], and biotemplate-directed sol-gel method [19,20]. Significantly, Wang et al. have presented the preparation of the SnO_2 nanotube arrays on titanium substrate via ZnO nanowire arrays as sacrificial templates [21]. Han et al. have reported the synthesis of SnO_2 octahedral nanoparticles by the poly (vinyl pyrrolidone) (PVP) assisted hydrothermal method [22], and Tan et al. have reported the synthesis of SnO_2 nanocrystal via a solid-state reaction method [23]. It is well known that the sensing mechanism of SnO_2 belongs to the surface-controlled type, in which the grain size, defect, and oxygen-adsorption quantity play important roles in sensing properties. In several recent reports, it has been shown that the sensing performance of sensor based on SnO_2 nanostructures strongly depend on the size, specific surface area, and morphology [24–27].

In our work, three-dimensional (3 D) SnO_2 hierarchical architectures were synthesized by a simple hydrothermal method. The obtained SnO_2 nanostructures consisted of a large number of single

* Corresponding authors. Tel.: +86 431 85167808; fax: +86 431 85167808.
E-mail addresses: liangxs@jlu.edu.cn (X. Liang), lugy@jlu.edu.cn (G. Lu).

0925-4005/$ – see front matter © 2012 Elsevier B.V. All rights reserved.
http://dx.doi.org/10.1016/j.snb.2012.11.043

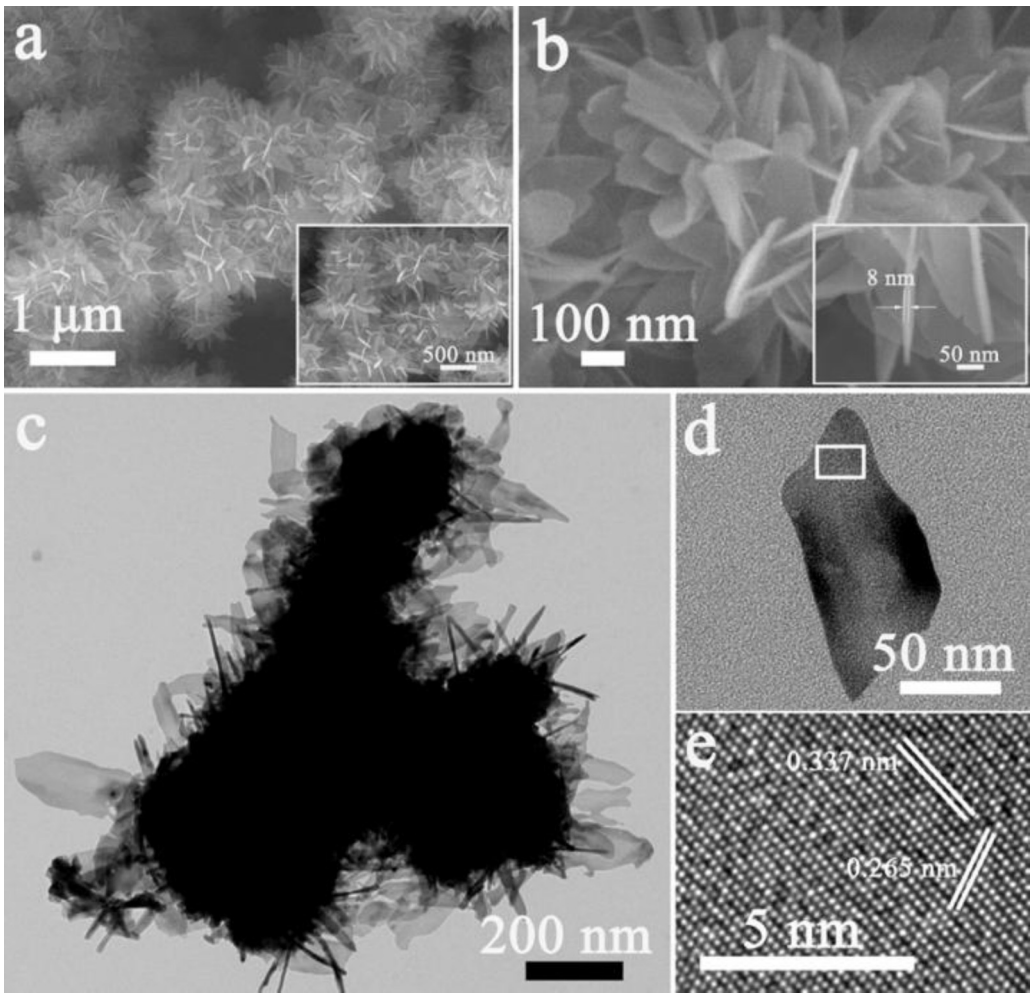

Fig. 1. (a and b) FESEM, (c and d) TEM images of the as-prepared SnO_2 product. The insets show high magnification FESEM images. (e) HRTEM image obtained from the marked fringe of nanosheet.

crystalline nanosheets. It was observed that the hydrochloric acid amount had a dramatic effect on both the size and morphology of the sample in present synthesis. A comparative gas sensing properties investigation between as-synthesized hierarchical SnO_2 nanosheets and conventional SnO_2 nanoparticles was performed to demonstrate the good gas sensing properties of the 3 D nanostructures.

2. Experimental

2.1. Synthesis and characterization of hierarchical SnO_2

All the reagents in the experiment were purchased from Beijing Chemical Reagent and used as received without further purification. In a typical experiment, stannous sulfate ($SnSO_4$, 0.1 g), trisodium citrate dehydrate ($Na_3C_6H_5O_7{\cdot}2H_2O$, 1.37 g), were dissolved in a glycerol-water solution with vigorous stirring to form a homogeneous solution. Then 0.3 mL hydrochloric acid (HCl 38%) solution was added in the above mixture. The reaction mixture was transferred into a Teflon-lined stainless-steel autoclave, kept at 180 °C for 24 h. After the hydrothermal procedure, the autoclave cooled down to room temperature naturally. Finally, the precipitates were collected by centrifugation, washed several times with deionized water and absolute ethanol, respectively, and dried in air at 80 °C.

The crystal structure of the as-prepared product was investigated by X-ray diffraction (XRD) (Rigaku TTRIII, with Cu Kα1 radiation). The morphology and microstructure were characterized by filed-emission scanning electron microscopy (FESEM, JEOL JSM-7500F, operated at an acceleration voltage of 15 kV). Transmission electron microscopy (TEM) and high-resolution transmission electron microscopy (HRTEM) measurements were obtained on a JEOL JEM-2100 microscope operated at 200 kV. The specific surface area was measured using the Brunauer-Emmett-Teller (BET) equation based on the nitrogen adsorption isotherm obtained with a Micromeritics Gemini VII apparatus (Surface Area and Porosity System). The sample was degassed under vacuum (1 mbar) at 250 °C for 10 h prior to the measurement.

2.2. Fabrication and measurement of gas sensor

Gas sensors were fabricated as follows: the as-synthesized hierarchical SnO_2 nanosheets were mixed with water to form slurry, and then coated on an alumina tube by a small brush to form a thick film, and the detailed fabrication has been described in the literatures [28,29]. The gas-sensing properties of the samples were evaluated with a RQ-2 gas-sensing characterization system. The measurement was processed by a static process: a given amount of the tested gas was injected into a closed glass chamber, and the sensor was put into the chamber for the measurement of the sensitive performance. The desired concentration of the test gas was

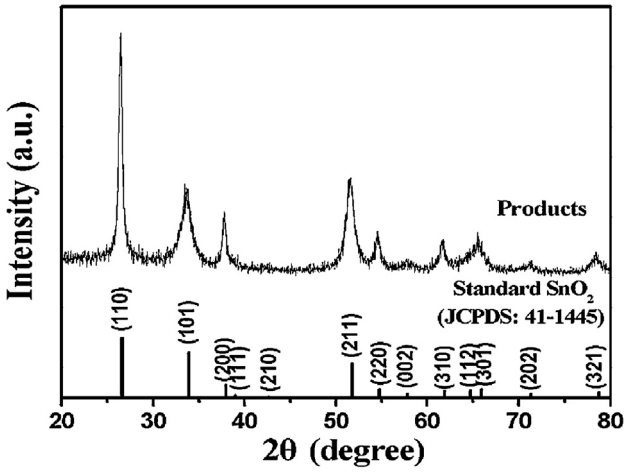

Fig. 2. XRD pattern of the as-prepared SnO_2 powder.

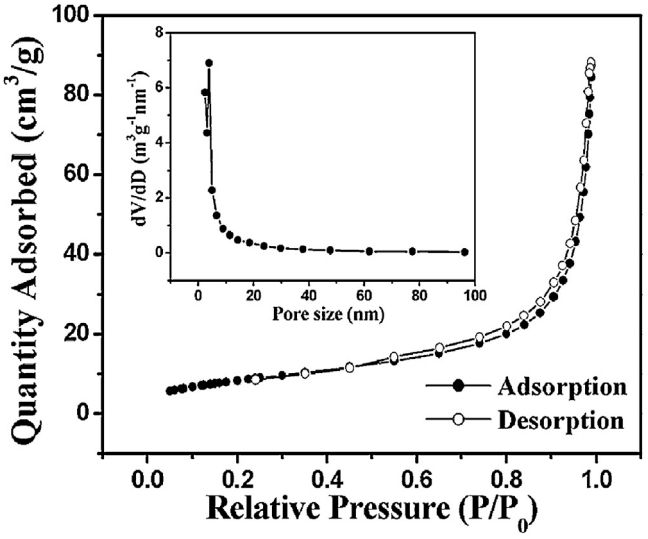

Fig. 3. Typical nitrogen adsorption-desorption isotherm and pore size distribution plot (inset) of the as-prepared SnO_2 product.

obtained by the static liquid gas distribution method, which was calculated by the following formula [30],

$$C = \frac{22.4 \times \phi \times \rho \times V_1}{M \times V_2} \times 1000 \quad (1)$$

where C (ppm) is the target gas concentration, φ the required gas volume fraction, ρ (g/mL) the density of the liquid, V_1 (μL) the volume of liquid, V_2 (L) the volume of the chamber, and M (g/mol) the molecular weight of the liquid. The gas response was defined as the ratio R_a/R_g, where R_a and R_g were the resistances measured in air and the tested gas atmosphere. The time of response and recovery were defined as the time taken by the sensor to achieve 90% of the total resistance change in the case of adsorption and desorption, respectively.

3. Results and discussion

The morphologies and microstructures of the as-prepared product were illustrated by FESEM observations. Flower-like nanostructures were clearly observed from a panoramic FESEM image (Fig. 1a). No other morphologies could be detected, indicating a high yield of these 3 D nanostructures. Moreover, it can be seen that the SnO_2 product had a uniform size of about 500 nm (the inset of Fig. 1a). The enlarged FESEM image of an individual SnO_2 with a hierarchical architecture, as shown in Fig. 1b, indicates that the flower-like nanostructures were constructed by many 2D nanosheets. The high-magnification FESEM image (the inset of Fig. 1b) shows the detailed morphological information of the nanosheets. It can be observed that the edge thickness of nanosheets was about 8 nm. In addition, the surface of the SnO_2 nanosheets was rather smooth. Further detailed morphological and structural analysis of the hierarchical nanosheets was carried out using transmission electron microscopy (TEM) and high-resolution transmission electron microscopy (HRTEM). The typical TEM image in Fig. 1c shows that the shape of product was similar to those of the FESEM observations. Fig. 1d presents the magnified TEM image of an individual SnO_2 nanosheet. The clear lattice fringes in the HRTEM image confirmed the single-crystalline nature of the nanosheet. The lattice fringe spacing was observed to be 0.337 and 0.265 nm (Fig. 1e). They were found to correspond to (110) and (101) planes of rutile SnO_2, respectively.

Fig. 2 shows the typical X-ray diffraction (XRD) pattern of the product prepared by hydrothermal process, from which all of the diffraction peaks were quite similar to those of bulk SnO_2, which can be indexed as the tetragonal rutile structure of SnO_2 with lattice constants of a = 4.738 Å and c = 3.187 Å. It was consistent with the standard data file (JCPDS file no. 41-1445). No diffraction peaks from any other impurities were observed, indicating the high purity of the product. Compared with those of the bulk material, the peaks were relatively broadened, which demonstrated that the SnO_2 had a small crystallite size. Using the Scherer equation ($D = 0.89\lambda/\beta\cos\theta$ where D is the crystallite size, λ the wavelength of X-ray, β the line broadening at full width half-maximum, and θ the Bragg diffraction angle of the peak) to calculate the crystallite size for the as-synthesized product indicated the mean crystallite size of about 10 nm. The calculated value almost accords with the thickness of nanosheet observed from the SEM (the inset of Fig. 1b) and TEM (Fig. 1c) images.

To analyze the surface structural characteristic of the as-synthesized SnO_2 nanostructures, nitrogen adsorption and desorption measurements were carried out. Fig. 3 presents the nitrogen adsorption and desorption isotherms and the corresponding Barret-Joyner-Halenda (BJH) pore size distribution plot (the inset of Fig. 3) of the product. As observed in Fig. 3, the hierarchical SnO_2 nanosheets exhibited a type IV isotherm with a type H3 hysteresis loop for the relative pressure P/P_0 in the range 0.5–1 [31], according to the IUPAC classification, which suggests the presence of mesoporous (2–50 nm) structure in the product [32]. Based on the BJH method and the adsorption branch of the nitrogen isotherm, the calculated pore-size distribution indicated that a correspondingly narrow pore size distribution centered at about 4 nm. The BET surface area of the product was calculated to be 31 m^2/g.

The influence of experimental parameter on the microstructures of final as-prepared products was investigated systemically. The result shows that the amount of HCl played an important role in controlling the size and morphology of the SnO_2 nanostructures. Keeping other conditions unchanged, in the absence of HCl, the resultant product consisted of flower-like nanostructures with a size of about 2 μm, as shown in Fig. 4a. The inset shows that the thickness of nanosheets was about 20–30 nm. With the introduction of HCl (0.1 mL) into the reaction system, the flower-like nanostructures were maintained. However, the size of product was reduced, from original 2 μm became current 1 μm (Fig. 4b). The thickness was also decreased to 10–15 nm, as shown in the inset of Fig. 4b. As the amount of HCl was increased to 0.3 mL, the morphology of product remained unchanged, the thickness was further reduced (Fig. 4c and the inset), the detailed structure characteristics of them have been described previously. Further increase of HCl (0.9 mL), the FESEM image indicates that these flower-like

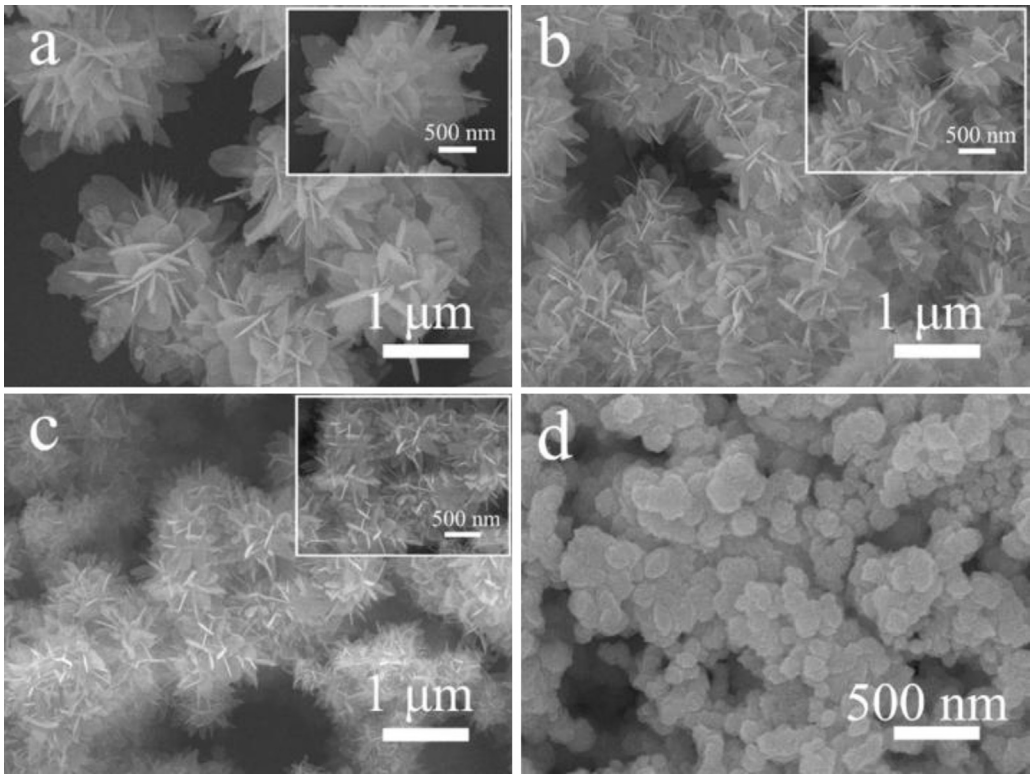

Fig. 4. FESEM images of product obtained with different HCl content: (a) 0.0, (b) 0.1, (c) 0.3, and (d) 0.9 mL. The insets show the enlarged FESEM images.

nanostructures transformed into the agglomerates with the size of about 100–200 nm, as shown in Fig. 4d. Therefore, on the basis of the morphological study, it can be concluded that HCl plays an important role in forming flower-like SnO_2 nanostructures and controlling their size.

Gas sensors have attracted a remarkable interest due to the growing concern on environmental monitoring and domestic/public safety. It was expected that such a unique structure of SnO_2 might bring about efficient sensing properties. It is well known that the response of a gas sensor is highly influenced by its operating temperature [33,34]. Firstly, the optimal operating temperatures of the sensor to different testing gases were investigated. Fig. 5 shows the response plots of the sensor towards 100 ppm C_2H_5OH, HCHO, and C_3H_6O at different operating temperature. It is obvious that the responses of the tested sensor varied with operating temperature. The response to C_2H_5OH rapidly increased and reached its maximum at the operating temperature of 275 °C, and then decreased with a further rise of the operating temperature. The same behavior was observed in the case of other test gases, and their maximum appeared at different temperature. The response of the sensor to C_2H_5OH reached the maximum value of 32.7 at 275 °C, which was about 8.4 and 4.5 times higher than the responses of HCHO and C_3H_6O obtained at the same temperature. This operating temperature of 275 °C could be useful for an improved selectivity of ethanol.

Then, the dynamic response characteristics of the sensor based on as-prepared SnO_2 hierarchical nanostructures to different gases were investigated. Fig. 6 displays the response o the sensor to 60 ppm C_2H_5OH, HCHO, and C_3H_6O at their corresponding optimal temperature of 275, 200, and 275 °C, respectively. It is obvious that the sensor showed sensitive and reversible response to these gases. Moreover, the sensor presents the rapid response and recovery to HCHO. However, the response of the sensor to either HCHO or C_3H_6O was lower than that to C_2H_5OH.

For comparison, two kinds of gas sensors were fabricated using the as-synthesized hierarchical SnO_2 nanosheets and SnO_2 nanoparticles synthesized conventionally. Fig. 7 presents a bar graph of the response of two kinds of gas sensors to 100 ppm ethanol at different operating temperature. Obviously, the sensor based on hierarchical SnO_2 nanosheets exhibited higher response to ethanol compared with that of sensor using nanoparticles at various temperatures. The result suggests that the as-synthesized 3 D hierarchical SnO_2 architectures had better gas sensing property and was a promising candidate for high performance ethanol

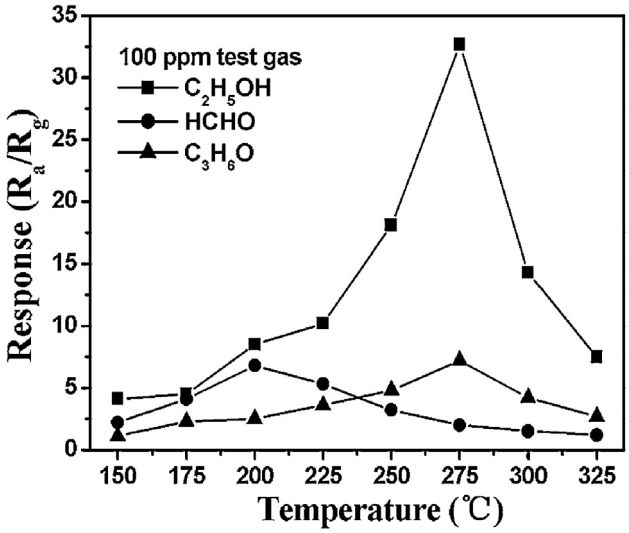

Fig. 5. Response of sensor using as-prepared SnO_2 nanostructures to 100 ppm C_2H_5OH, HCHO, and C_3H_6O as a function of the operating temperature, respectively.

sensor. Moreover, two kinds of sensors had the same optimal operating temperature, at which the sensor showed the highest response.

Selectivity is an important parameter of a gas sensor. Fig. 8 shows a bar graph of the response of two sensors to a variety of gases, such as ethanol, acetone, CO, etc. All of the gases were tested at an operating temperature of 275 °C with a concentration of 100 ppm. As expected, the sensor based on hierarchical SnO_2 nanosheets showed enhanced responses to gas compared with that of nanoparticles. Moreover, the results indicate that the sensor exhibited the highest response to ethanol among the tested gas and the response was about 32.7. The response towards toluene was no greater than 2. Therefore, it was concluded that the sensor using as-synthesized hierarchical SnO_2 nanosheets showed selectivity toward ethanol as oppose to any other gas.

The relationship between response and ethanol concentrations for the sensor at operating temperatures of 275 °C is displayed in Fig. 9. From the curve, it is found that the responses of sensor increased with the gas concentrations. Moreover, the responses were proportional to the increasing concentrations of ethanol, when the gas concentrations were correspondingly low. Above 400 ppm, the responses increased slowly with the gas concentrations, which indicated that the sensor tended to saturation gradually. The inset of Fig. 9 shows that the increase in the responses depends near linearly on the gas concentrations in the range from 40 to 100 ppm for the sensor.

Response and recovery time are also important parameters of a gas sensor, Fig. 10 shows the response transients of sensor to 60 ppm ethanol at 275 °C, and the results indicate that the hierarchical SnO_2 sensor had a fast response-recovery process. The response and recovery time of the sensor based on the as-prepared SnO_2 hierarchical structures were about within 11 and 125 s, respectively. The three reversible cycles of the response curve indicated a stable and repeatable characteristic, as shown in the inset of Fig. 10.

The response and recovery characteristics were further investigated with the sensor being orderly exposed to different concentration at 275 °C. It can be seen that the characteristics of response and recovery were almost reproducible with the quick

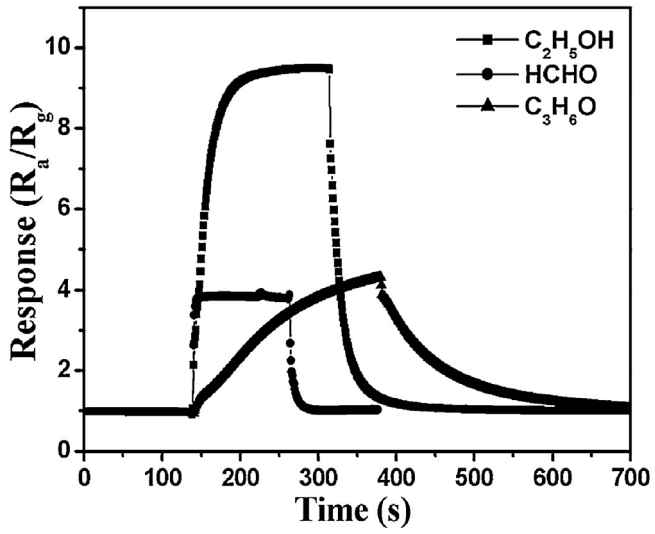

Fig. 6. Response of the sensor towards 60 ppm C_2H_5OH, HCHO, and C_3H_6O, respectively.

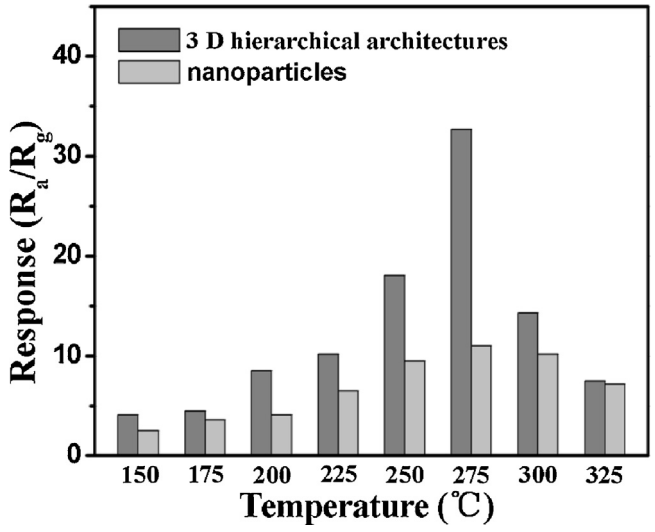

Fig. 7. Response of two sensors to 100 ppm ethanol as a function of the operating temperature.

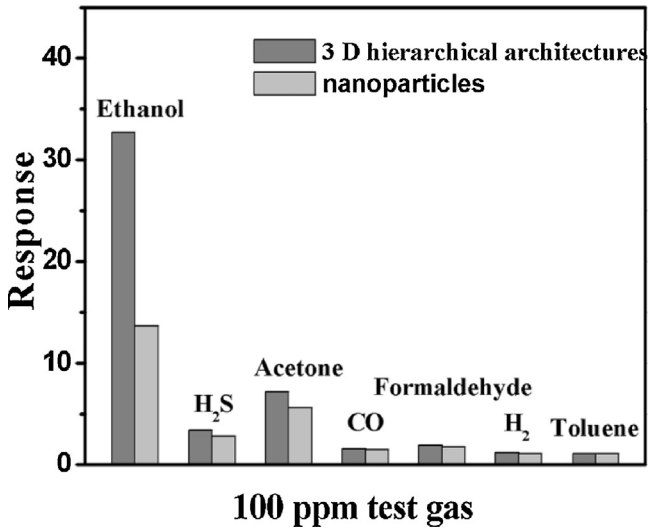

Fig. 8. Response of sensors based on as-prepared 3D SnO_2 nanostructures and SnO_2 nanoparticles to various gases at 275 °C.

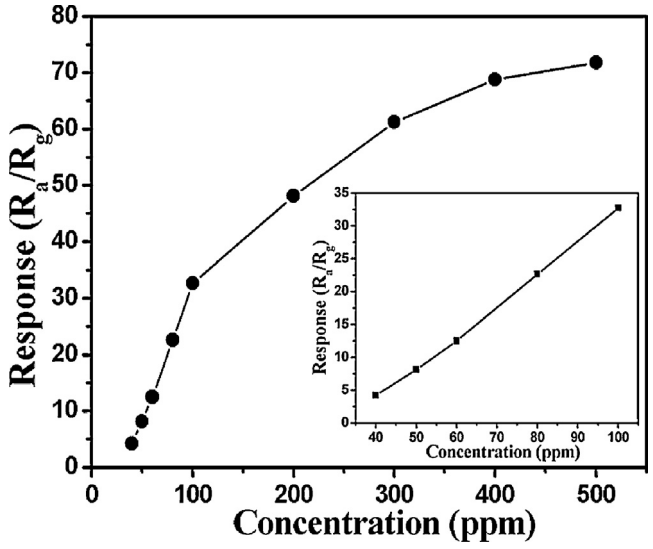

Fig. 9. Response of the sensor using 3 D SnO_2 nanostructures versus ethanol concentrations at 275 °C. The inset shows the linear concentration dependence of response in the range of 40-100 ppm.

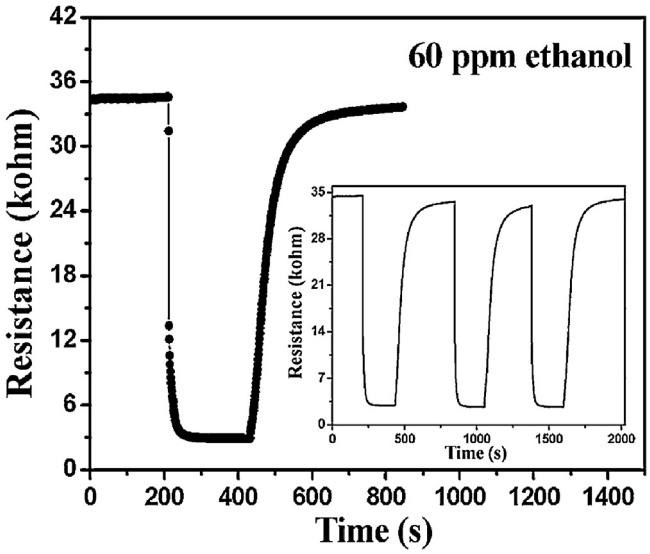

Fig. 10. Response transients of the sensor to 60 ppm ethanol at 275 °C. The inset displays three periods of response curve.

time of response and recovery. This almost square response shape observed indicated that the sensor responded rapidly to test gas, quickly achieving a near steady state. Then the resistance of sensor changed slowly due to test gas diffusing through the material and occupying the remaining surface reaction sites. When the sensor was exposed to air, the resistance returned to near baseline level. The response was about 4.2, 8.1, 12.5, and 17.6 to 40, 50, 60 and 70 ppm ethanol, respectively, as shown in Fig. 11.

The sensing mechanism of metal oxides gas sensors has been clarified in previous works [35–37]. The most widely accepted theory is based on the change in resistance of the sensor upon exposure to different gas atmospheres. When the sensor is exposed to air, oxygen molecules adsorb onto the surfaces of nanosheets, and form chemisorbed oxygen species by capturing electrons from the conductance band of SnO_2. The decrease of the electron concentration in the conduction band leads to stabilization of high resistance. When the sensor is exposed to ethanol, CO, or other reductive gas atmospheres at a moderate temperature, these gas molecules will react with the adsorbed oxygen species on the surface of SnO_2 nanosheets. This process releases the trapped electrons back to the

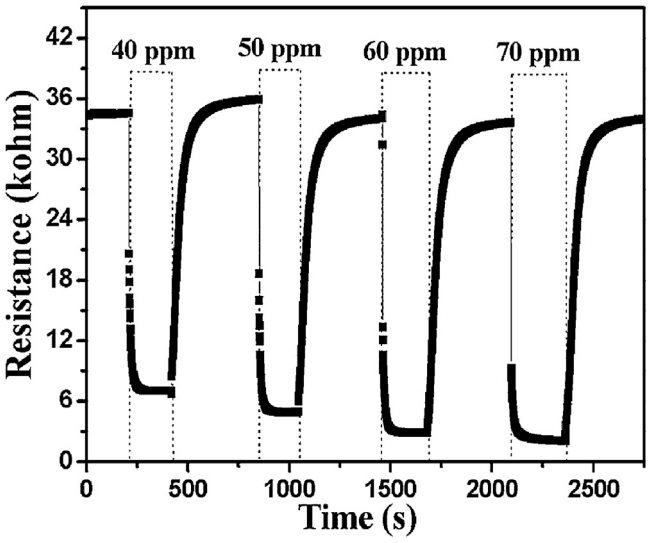

Fig. 11. Response transients of the sensor to different concentrations of ethanol.

conductance band of SnO_2 and results in an increase the electron concentration. This effect eventually increases the conductivity of the SnO_2 nanosheets.

The enhancement in gas-sensing property on hierarchical SnO_2 architectures may be ascribed to their unique architectures. It is well known that the effort to enhance the gas response by decreasing the particle sizes down to a scale of several nanometers is counteracted by the formation of aggregates due to Van der Waals attraction. The diffusion of target gas into the inner part of secondary aggregates is ineffective because of the small pore, long diffusion length, and tortuous pathway. This is the main reason for the low gas response in the aggregated nanoparticles. In contrast, the hierarchical structures provide well-defined and well-aligned micro-, and nanoporosity for effective gas diffusion. In other word, the utility factor of the sensing body is enhanced. Moreover, the thickness of nanosheets (8 nm) reaches to a scale comparable with the electron depletion layer thickness, thus complete depletion will be achieved. Therefore, a high gas response can be obtained using hierarchical nanostructures.

4. Conclusions

In summary, a simple one-step solution route was reported for the formation of 3 D SnO_2 nanostructure with hierarchical structure, which were composed of many 2D nanosheets with the thickness of about 8 nm. The amount of HCl exerted crucial influence on the final size and morphology. Comparative gas sensing tests between sensors based on as-prepared SnO_2 hierarchical architectures and SnO_2 nanoparticles clearly displayed that the former showed more excellent sensing performances. The enhanced gas sensing performances were attributed to the unique hierarchical structure.

Acknowledgements

This work was supported by the Natural Science Foundation of P. R. China under Grant Nos. 61006055, 61074172, 61134010 and Program for Chang Jiang Scholars, and Innovative Research Team in University (No. IRT1017). Project (20121105) Supported by Graduate Innovation Fund of Jilin University.

References

[1] N. Yamazoe, New approaches for improving semiconductor gas sensor, Sensors and Actuators B 5 (1991) 7–19.
[2] S.C. Naisbitt, K.F.E. Pratt, D.E. Williams, I.P. Parkin, A microstructural mode of semiconducting gas sensor response: the effects of sintering temperature on the response of chromium titanate (CTO) to carbon monoxide, Sensors and Actuators B 114 (2006) 969–977.
[3] Q. Tang, W.J. Zhou, W. Zhang, S.M. Ou, K. Jiang, W.C. Yu, Y.T. Qian, Size-controllable growth of single crystal $In(OH)_3$ and In_2O_3 nanocubes, Crystal Growth and Design 5 (2005) 147–150.
[4] G. Korotcenkov, A. Cerneavschi, V. Brinzari, A. Vasiliev, M. Ivanov, A. Cornet, J. Morante, A. Cabot, J. Arbiol, In_2O_3 films deposited by spray pyrolysis as a material for ozone gas sensors, Sensors and Actuators B 99 (2004) 297–303.
[5] (a) Y.J. Chen, L. Nie, X.Y. Xue, Y.G. Wang, T.G. Wang, Linear ethanol sensing of SnO2 nanorods with extremely high sensitivity, Applied Physics Letters 88 (2006) 083105;
(b) X.Y. Xue, Y.J. Chen, Y.G. Liu, S.L. Shi, Y.G. Wang, T.G. Wang, Applied Physics Letters 88 (2006) 201907.
[6] K.M. Li, Y.J. Li, M.Y. Lu, C.I. Kuo, L.J. Chen, Direct conversion of single-layer SnO nanoplates to multi-layer SnO_2 nanoplates with enhanced ethanol sensing properties, Advanced Functional Materials 19 (2009) 2453–2456.
[7] U. Ciesla, F. Schuth, Ordered mesoporous materials, Microporous and Mesoporous Materials 27 (1999) 131–149.
[8] P. Yang, D. Zhao, D.I. Margolese, B.F. Chmelka, G.D. Stucky, Generalized syntheses of large-pore mesoporous metal oxides with semicrystalline frameworks, Nature 396 (1998) 152–155.
[9] J.K. Shon, S.S. Kong, Y.S. Kim, J.-H. Lee, W.K. Park, S.C. Park, J.M. Kim, Solvent-free infilteration method for mesoporous SnO_2 using mesoporous silica templates, Microporous and Mesoporous Materials 120 (2009) 441–446.
[10] A. Kolmakov, Y. Zhang, G. Cheng, M. Moskovits, Detection of CO and O_2 using tin oxide nanowire sensors, Advanced Materials 15 (2003) 997–999.

[11] V.V. Sysoev, B.K. Button, K. Wepsiec, S. Dmitriev, Toward the nanoscopic electronic nose: hydrogen vs carbon monoxide discrimination with an array of individual metal oxide nano- and mesowire sensors, Nano Letters 6 (2006) 1584–1588.
[12] A. Kay, M. Grätzel, Dye-sensitized core-shell nanocrystals: improved efficiency of mesoporous tin oxide electrodes coated with a thin layer of an insulating oxide, Chemistry of Materials 14 (2002) 2930.
[13] S. Gubbala, V. Chakrapani, V. Kumar, M.K. Sunkara, Band-edge engineered hybrid structures dye-sensitized solar cells based on SnO_2 nanowires, Advanced Functional Materials 18 (2008) 2411–2418.
[14] Y.S. Lin, J.G. Duh, M.H. Huang, Shell-by-shell synthesis and applications of carbon-coated SnO_2 hollow nanospheres in lithium-ion battery, Journal of Physical Chemistry C 114 (2010) 13136–13141.
[15] S. Sun, G. Meng, G. Zhang, J.P. Masse, L. Zhang, Controlled growth of SnO_2 hierarchical nanostructures by a multistep thermal vapor deposition process, Journal of European Chemistry 13 (2007) 9087–9092.
[16] H. Ohgi, T. Maeda, E. Hosono, S. Fujihara, H. Imai, Evolution of nanoscale SnO_2 grains, flakes, and plates into versatile particles and films through crystal growth in aqueous solutions, Crystal Growth and Design 5 (2005) 1079–1083.
[17] G. Cheng, K. Wu, P. Zhao, Y. Cheng, X. He, K. Huang, Controlled growth of oxygen deficient tin oxide nanostructures via a solvothermal approach in mixed solvents and their optical properties, Nanotechnology 18 (2007) 355604.
[18] X.W. Lou, Y. Wang, C.L. Yuan, J. Yang, L.A. Archer, Template-free synthesis of SnO_2 hollow nanostructures with high lithium storage capacity, Advanced Materials 18 (2006) 2325–2329.
[19] Q. Dong, H. Su, D. Zhang, F. Zhang, Fabrication and gas sensitivity of SnO_2 hierarchical films with interwoven tubular conformation by a biotemplate-directed sol-gel technique, Nanotechnology 17 (2006) 3968–3972.
[20] Q. Dong, H. Su, J. Xu, D. Zhang, Influence of hierarchical nanostructures on the gas sensing properties of SnO_2 biomorphic films, Sensors and Actuators B 123 (2007) 420–428.
[21] J.Z. Wang, N. Du, H. Zhang, J.X. Yu, D.R. Yang, Large-scale synthesis of SnO_2 nanotube arrays as high-performance anode materials of Li-ion batteries, Journal of Physical Chemistry C 115 (2011) 11302–11305.
[22] X.G. Han, M.S. Jin, S.F. Xie, Q. Kuang, Z.Y. Jiang, Y.Q. Jiang, Z.X. Xie, L.S. Zheng, Synthesis of tin dioxide octahedral nanoparticles with exposed high-energy {221} facets and enhanced gas-sensing properties, Angewandte Chemie International Edition 48 (2009) 9180–9183.
[23] E.T.H. Tan, G.W. Ho, A.S.W. Wang, S. Kawi, A.S.T. Wee, Gas sensing properties of tin oxide nanostructures synthesized via a solid-state reaction method, Nanotechnology 19 (2008) 255706.
[24] J. Zhang, S.R. Wang, Y. Wang, M.J. Xu, H.J. Xia, S.M. Zhang, W.P. Huang, X.Z. Guo, S.H. Wu, Facile synthesis of highly ethanol-sensitive SnO_2 nanoparticles, Sensors and Actuators B 139 (2009) 369–374.
[25] J.Q. Xu, D. Wang, L.P. Qin, W.J. Yu, Q.Y. Pan, SnO_2 nanorods and hollow spheres: controlled and gas sensing properties, Sensors and Actuators B 137 (2009) 490–495.
[26] S.C. Yeow, W.L. Ong, A.S.W. Wong, G.W. Ho, Template-free synthesis and gas sensing properties of well-controlled porous tin oxide nanospheres, Sensors and Actuators B 143 (2009) 295–301.
[27] H.T. Chen, S.J. Xiong, X.L. Wu, J. Zhu, J.C. Shen, Tin oxide nanoribbons with vacancy structures in luminescence-sensitive oxygen sensing, Nano Letters 9 (2009) 1926–1931.
[28] P. Sun, Y. Cao, J. Liu, Y.F. Sun, J. Ma, G.Y. Lu, Dispersive SnO_2 nanosheets: hydrothermal synthesis and gas-sensing properties, Sensors and Actuators B 156 (2011) 779–783.
[29] P. Sun, L. You, D.W. Wang, Y.F. Sun, J. Ma, G.Y. Lu, Synthesis and gas sensing properties of bundle-like α-Fe_2O_3 nanorods, Sensors and Actuators B 156 (2011) 368–374.
[30] H.T. Fan, Y. Zeng, H.B. Yang, X.J. Zheng, L. Liu, T. Zhang, Preparation and gas sensitive properties of ZnO-CuO nanocomposites, Acta Physico-Chimica Sinica 24 (2008) 1292–1296.
[31] M. Kruk, M. Jaroniec, Gas adsorption characterization of ordered organic-inorganic nanocomposite materials, Chemistry of Materials 13 (2001) 3169–3183.
[32] Y.G. Sun, B. Gates, B. Mayers, Y.N. Xia, Crystalline silver nanowires by soft solution processing, Nano Letters 2 (2002) 165–168.
[33] V.R. Shinde, T.P. Gujar, C.D. Lokhande, Enhanced response of porous ZnO nanobeads towards LPG: Effect of Pd sensitization, Sensors and Actuators B 123 (2007) 701–706.
[34] Z. Cao, J.R. Stetter, A selective solid-state gas sensor for halogenated hydrocarbons, Sensors and Actuators B 1-4 (1991) 109–113.
[35] N. Yamazoe, G. Sakai, K. Shimanoe, Oxide semiconductor gas sensors, Catalysis Surveys from Asia 7 (2003) 63–75.
[36] M. Egashira, Y. Shimizu, Y. Takao, S. Sako, Variations in I-V characteristics of oxide semiconductors induced by oxidizing gases, Sensors and Actuators B 35 (1996) 62–67.
[37] Y. Min, H.L. Tuller, S. Palzer, J. Wölenstein, H. Bötner, Gas response of reactively sputtered ZnO films on Si-based micro-array, Sensors and Actuators B 93 (2003) 435–441.

Biographies

Peng Sun received his MS degree from State Key Laboratory of Superhard Materials, Jilin University, China in 2009. He entered the PhD course in 2010, majoring in microelectronics and solid state electronics. Now, he is engaged in the synthesis and characterization of the semiconducting functional materials and gas sensors.

Xiaodong Mei received her BS degree from the Electronics Science and Engineering department, Jilin University, China in 2012. Presently, she is a graduate student, majored in circuits and systems.

Yaxin Cai obtained her BS degree from the Electronics Science and Engineering college, Jilin University, China in 2012. She current research interest is the synthesis of functional materials.

Jian Ma received his MS in 2009 from Jilin University at the Electronics Science and Engineering department. Presently, he is working as Technical Assistant in Electronics Science and Engineering department. His current research interests are gas sensor, the design and fabrication of micro-hot plates.

Yanfeng Sun obtained his PhD from Jilin University of China in 2007. Presently, he is working as Lecturer in Electronics Science and Engineering department of Jilin University. His current research interests are nanoscience and gas sensors.

Xishuang Liang received the B.Eng. degree in Department of Electronic Science and Technology in 2004. He received his Doctor's degree in College of Electronic Science and Engineering at Jilin University in 2009. Now he is a lecturer of Jilin University, China. His current research is solid electrolyte gas sensor.

Fengmin Liu received the BE degree in Department of Electronic Science and Technology in 2000. She received her Doctor's degree in College of Electronic Science and Engineering at Jilin University in 2005. Now she is an associate professor in Jilin University, China. Her current research is preparation and application of semiconductor oxide, especial in gas sensor and solar cell.

Geyu Lu received his BS and MS degree in electronic sciences from Jilin University, China in 1985 and 1988, respectively, and PhD degree in 1998 from Kyushu University in Japan. Now he is a professor of Jilin University, China. Presently, he is interested in the development of functional materials and chemical sensors.